PRAMANA — journal of physics

Vol. 82, No. 1
January 2014
pp. 111–120

Probing strong field ionization of solids with a Thomson parabola spectrometer

MALAY DALUI[1], T MADHU TRIVIKRAM[1], RAM GOPAL[2] and M KRISHNAMURTHY[1,2,*]

[1]Tata Institute of Fundamental Research, Dr Homi Bhabha Road, Mumbai 400 005, India
[2]TIFR Centre for Interdisciplinary Sciences, 21 Brundavan Colony, Narsingi, Hyderabad 500 075, India
*Corresponding author. E-mail: mkrism@tifr.res.in

DOI: 10.1007/s12043-013-0648-7; ***e*Publication:** 11 January 2014

Abstract. Intense ultrashort laser pulses are known to generate high-density, high-temperature plasma from any substrate. Copious emission of hot electrons, from a solid substrate, results in strong electrostatic field that accelerates the ions with energies ranging from a few eV to MeV. Ion spectrometry from laser–plasma is convolved with multiple atomic systems, several charge states and a broad energy spread. Conventional mass spectrometric techniques have serious limitations to probe this ionization dynamics. We have developed an imaging ion spectrometer that measures charge/mass-resolved ion kinetic energies over the entire range. Microchannel plate (MCP) is used as the position-sensitive detector to perform online and single shot measurements. The well-resolved spectrum even for the low-energy ions, demonstrates that the spectral width is limited by the space-charge repulsion for the ions generated in the hot dense plasma.

Keywords. Ion acceleration; Thomson parabola spectrometer; laser–plasma.

PACS Nos 52.38.Kd; 52.38.−r; 07.77.Ka; 29.40.Gx

1. Introduction

Recent developments in laser technology enables us with ultrashort high intensity lasers that generate peak intensity up to 10^{22} W/cm^2 on a table top [1]. The interaction of such lasers with matter instantly generates plasma at solid-like density and temperatures that are orders of magnitude larger than plasmas generated in conventional techniques [2]. The complex mixture of high-energy electrons and ions can be tailored to accelerate ions, electrons, neutral atoms [3] or even negative ions [4]. The nature of initial matter that absorbs light and the laser parameters decisively changes the way in which matter absorbs the laser energy. The dynamics of ionization in the plasma is widely different depending on these parameters and the absorbed energy is channelled very differently in the course of

plasma evolution. When low-density gases are probed with optimum laser pulse duration and energy, plasma wake fields are generated that accelerate electrons to GeVs through wake-field acceleration schemes [5]. Short-intense burst of light incident on the solid substrate accelerates ions to multi-MeV [6,7] via target-normal sheath acceleration (TNSA) mechanism [8]. Since the plasma is created by an ultrashort burst of light, the source of electrons or ions intrinsically have an ultrashort time duration (few picoseconds). Such laser-accelerated ion source has very high peak current, broad energy spectrum and very small source size (few microns) [9]. Laser-driven ion acceleration becomes a very rapidly growing research field with potential application in proton therapy [10], relativistic ion beam production [11], laboratory astrophysics and high-energy density science [12]. Due to its lighter mass, electrons respond to the electric field of the light pulse instantly and the large electric field drives the electrons to a very high energy. These hot electrons quickly move out of the solid surface, long before the ions move and the electron drift creates a strong quasistatic charge separation sheath electric field. Ions are then accelerated in this sheath field preferentially along the target normal direction. The acceleration mechanism can be explained by considering a plasma expanding into the vacuum [13–15]. Protons are always detected in such experiments, regardless of the chemical composition of the solid substrate, as a thin layer of hydrocarbon or water is always present as surface contaminant. Owing to its highest charge-to-mass ratio (q/m) among the ions, protons get the maximum acceleration and shield the sheath field for other ions.

Deciphering the charge of the ions of different species constituting the plasma and measuring the energy of different ion constituents are the most important steps in the study of ionization dynamics. The simplest method to study ion emission is to measure the time-of-flight (TOF) of the ions [16,17]. Typically in a TOF measurement, the detector records the arrival time of the particles impinging on it. It returns a current pulse whose horizontal axis contains the arrival time information of the ions and the vertical axis or the current amplitude is proportional to the incident particle flux. It is easy to get the ion energy from the arrival time if the mass is provided, assuming ballistic ion propagation. However, if the ions are not monoenergetic, TOF method can distinguish neither generation of different atomic species nor their charge states. In laser–solid interactions, where the ion energies are widely distributed (eV to MeV) and a plethora of charge states are possible for all atomic constituents, the TOF signals are badly convolved and very little information is discernible. To avoid such complications and to know the ionization dynamics in more detail, it is inevitable to use Thomson parabola spectrometer (TPS). TPS is widely used to characterize laser-accelerated ions in multi-MeV energy range [18–20]. However, TPS cannot be used to characterize relatively low-energy ions (1–100 keV) because of its inherently poor charge state resolution due to space-charge effect.

We report the design and development of a Thomson parabola spectrometer, which can resolve low-energy ions. Such spectrometers are usually equipped with CR-39, image-plate, radiochromic film (RCF) etc. as the position-sensitive ion detector. These detectors do not show the ion image instantly. The data are acquired for a few laser shots and processed after the experiment. For high repetition rate laser experiments, the ability to instantly observe the ion image is crucial to ensure that optimum experimental parameters are maintained in the course of the experiment. We use a microchannel plate (MCP) as the position-sensitive detector to characterize ions in laser–solid interactions. We present the experiments carried out on ionization with aluminum substrate using a 40 fs pulse

focussed at an intensity of 4×10^{17} W/cm^2. We present well-resolved TPS ion spectra for the low-energy ions, where the charge resolution is generally poor. We show that the trace width of the parabolic ion traces is limited only by the space-charge width. Since the ions originate in the high dense plasma, it is understandable that the trace widths are space-charge limited.

2. The Thomson parabola spectrometer: Working principle

Thomson parabola spectrometer distinctively disperses charged particles according to the charge-to-mass ratio (q/m) from a broad distribution of multiply charged species. It essentially maps the kinetic energy distribution of an ion (M^{q+}) into a parabolic trace in space. A position-sensitive detector, placed perpendicular to the ion propagation, would be able to capture the spatial distribution of the ions. TPS consists of parallel electric and magnetic field arrangements and oriented perpendicular to the ion velocity. Figure 1 shows the basic construction of a TPS. Ions, extracted through the aperture, get deflected in the field region (length L) and then continue drifting with constant velocity in the field-free region (length d) [21]. The motion of ion in the field region of the TPS is governed by the Lorentz force equation

$$\vec{F} = q(\vec{E} + \vec{v} \times \vec{B}), \tag{1}$$

where the electric and the magnetic fields are along the X-direction and the ion velocity is along the Z-direction, i.e. $\vec{E} = E\vec{x}$, $\vec{B} = B\vec{x}$ and $\vec{v} = v_z\vec{z}$.

For a positively charged ion propagating along the Z-direction, the electric field exerts a force along the X-direction and the magnetic field deflects it along the Y-direction. Two mutually perpendicular forces result in a parabolic ion trajectory in the X–Y plane. If the drift time of the ion in the field region and in the field-free region of the TPS are t_1 and t_2 respectively, then

$$t_1 = \frac{L}{v_z} \quad \text{and} \quad t_2 = \frac{d}{v_z}.$$

The transverse trajectory and velocity of the ion immediately after the field region of the TPS can be obtained by integrating eq. (1) and is given by

$$\vec{r}_\perp = \frac{q}{2m} t_1^2 (E\vec{x} + v_z B\vec{y}) \tag{2}$$

$$\vec{v}_\perp = \frac{q}{m} t_1 (E\vec{x} + v_z B\vec{y}). \tag{3}$$

Using the above equations, the deflection suffered by the test ion when it propagates through the TPS can be easily calculated. Ions with higher (lower) velocity spend less (more) time and suffer lesser (larger) deflection. The amount of deflection is proportional to the ion velocity or its kinetic energy. Equation (2) provides the deflection in the field region of the TPS as follows:

$$X_1\vec{x} + Y_1\vec{y} = \frac{qEL^2}{2mv_z^2}\vec{x} + \frac{qBL^2}{2mv_z}\vec{y}. \tag{4}$$

After the field region, the ion moves with a constant velocity $(\vec{v}_\perp, v_z)$ resulting in a field-free drift given below:

$$X_2\vec{x} + Y_2\vec{y} = \frac{qELd}{mv_z^2}\vec{x} + \frac{qBLd}{mv_z}\vec{y}. \tag{5}$$

So, the total ion deflection in the X–Y plane is $X = X_1 + X_2$ and $Y = Y_1 + Y_2$

$$X = \frac{qE}{2mv_z^2}L(L + 2d), \quad Y = \frac{qB}{2mv_z}L(L + 2d). \tag{6}$$

The equation of the ion trajectory is then given by

$$Y^2 = \frac{qB^2}{mE}L\left(\frac{L}{2} + d\right)X. \tag{7}$$

The ion trajectory is parabolic and contains charge (strictly q/m) resolved kinetic energy information. Each parabola belongs to a distinct charge-to-mass ratio. Photons and neutral particles, which cannot be deflected in the field of the TPS, constitute the origin $(X = 0, Y = 0)$ of the parabola. Along a parabola, the energy of the ions gradually decreases from the origin towards the edge of the detector. The kinetic energy (ε) of the ions can be calculated by setting $\varepsilon = \frac{1}{2}mv_z^2$ as follows:

$$\varepsilon = \frac{qE}{2X}L\left(\frac{L}{2} + d\right). \tag{8}$$

3. Experimental set-up

Figure 1 shows the schematic of the experimental system. A Ti:Sapphire 800 nm, 40 fs, CPA laser, capable of delivering 500 mJ energy at 10 Hz repetition rate, guided by two dielectric mirrors (M_1 and M_2) is focussed using an off-axis parabolic mirror (OAP) onto a solid target. The target is mounted on an x–y–z–θ motorized stage assembly, which enables the target to move during laser shots. The entire system is kept in a vacuum chamber maintained at a base pressure of 10^{-5} Torr. The TPS is housed in a separate vacuum chamber and pumped differentially to maintain a base pressure of 10^{-7} Torr to protect the MCP from laser–plasma debris. The energetic ions preferentially accelerated along the target normal (along the Z-axis) are extracted through a 100 μm aperture. This ensures a pencil-like ion beam of negligible transverse velocity $(v_z \gg v_x, v_y)$ in the field region of the TPS and also shield the MCP from X-rays. Two 12 cm long metal plates, kept 11 mm apart in the vacuum chamber, are used to produce the electric field. A pair of permanent magnets, kept outside along the electrodes, produces the magnetic field. A two-stage MCP, having a gain of about 10^7 kept at a distance of 1 m from the laser focus is used to record the ion tracks. A CCD camera equipped with necessary imaging optics images the fluorescence of the phosphor screen of the MCP.

In most of the TPS, the ion trajectories are stored permanently on the surface of the detector (CR-39 or RCF). An ion beam, upon impinging on these detectors, damages the surface and creates tracks. The read out is offline and takes 2–3 h. Such methods are better suited for single-shot experiments with lasers of low repetition rate where the time delay between the pulses is mandatorily in tens of minutes. Moreover, these offline

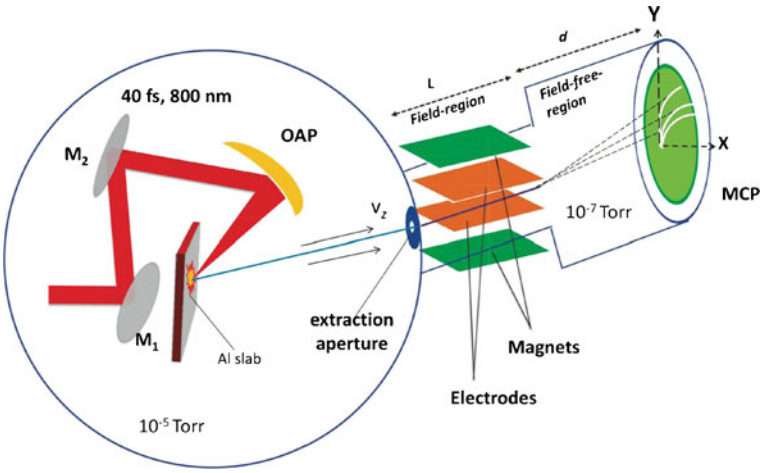

Figure 1. Schematics of the Thomson parabola spectrometer (TPS) and the experimental set-up: The *p*-polarized, 800 nm, 40 fs laser is focussed on an Al-slab yielding a peak intensity of 4×10^{17} W/cm^2. The TPS is kept along the target normal direction (*Z*-direction) in a differentially pumped, separate vacuum chamber, maintained at 10^{-7} Torr pressure. The distance from the laser focus to the microchannel plate (MCP) detector is 102 cm. The length of the field region and the field-free region of the TPS are respectively 15 cm and 25 cm.

detectors have a lower detection threshold in terms of ion energy. For laser of higher repetition rate (10 Hz or more) these are used by exposing the spectrometer to the laser plasma for a few shots and then the experiment is suspended for offline reading of the data. However, MCP allows online measurement. The advantage of instantly reading the ion image for each laser shot is enormous in the high repetition rate laser experiments. Unlike the particle track detectors, the use of MCP in the current experiment enables us to detect low-energy ions (down to eV). The spectrometer is optimized to probe low-energy ions, to develop the system with very good charge resolution even for low-energy ions. This provides us an explanation of ionization dynamics in the regime where it is hardly explored.

4. Results

A typical TPS trace of aluminum irradiated at 4×10^{17} W/cm^2 laser intensity is shown in figure 2a. In all laser–solid interactions, protons are always present as hydrocarbon or water contamination on the target surface unless special techniques are used to remove the contamination layer. Along with the proton we observe six ion traces of Al. Figure 2b shows the relative ion yield or the ion charge states propensity distribution (ICSPD). Beyond Al^{3+}, the ion yield is noted to decrease. The ionization potentials of Al are listed in table 1.

We notice that the ionization potential of Al^{2+} is 28.45 eV and next level of ionization for Al^{3+} is very hard as the ionization potential increases to 119.99 eV. So, the relative

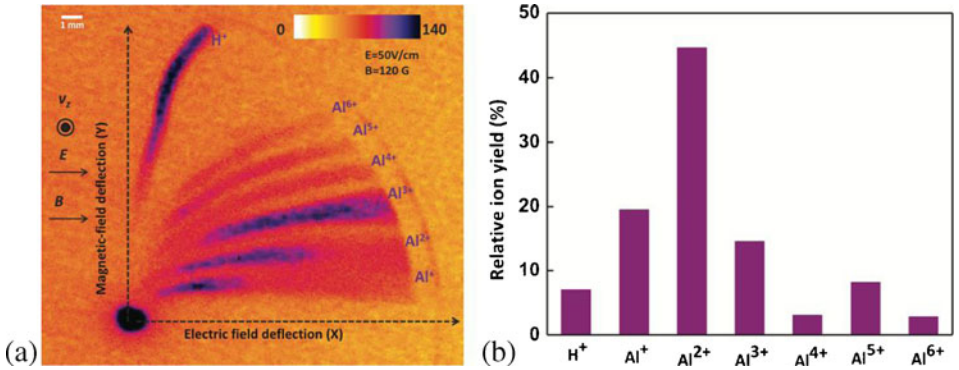

Figure 2. (**a**) A typical TPS image obtained when the laser irradiates an aluminum slab. The electric and the magnetic fields are applied along the *X*-direction, perpendicular to the ion velocity, which is along the *Z*-direction. Visible and invisible photons unaffected by the electromagnetic fields of the TPS, are incident on the MCP and create a central bright spot which constitutes the origin of the parabolic ion traces. The ion traces seem to become broader and tend to overlap towards the edge of the detector (away from the origin) because of space-charge effect. (**b**) Ion charge state propensity distribution of aluminum derived from the TPS image.

ion yield beyond Al^{3+} is very small and the average charge of the accelerated ions is 2.6. A solid substrate exposed to intense laser pulses generates much lower charge states than that formed in solid-density nanoclsuters [21]. Absence of continuous matter in these nanoclusters results in much larger charge density as the laser pulse drives the electrons and there is no return electron currents from the substrate unexposed to the laser pulses. More the ionization, larger is the further ionization by the laser-driven electrons both due to the collisional interaction and ionization ignition [22].

The femtosecond laser pulse incident on a solid target also couples energy directly to the electrons. Ions, because of their inertia cannot respond at that short time-scale (few tens of fs). At times much larger than the pulse duration, the hot electrons expand into the vacuum and create a quasistatic charge separation sheath electric field. The sheath field is given by [13]

$$E_{\text{sheath}} = \sqrt{\frac{2k_{\text{B}}n_{\text{eh}}T_{\text{eh}}}{e\varepsilon_0}}, \tag{9}$$

Table 1. Ionization potentials (IP) of Al. I, II and III denote first, second, third IP. These data are downloaded from http://www.nist.gov/.

Atomic state	IP (eV)	Atomic state	IP (eV)
Al I	5.99	Al IV	119.99
Al II	18.83	Al V	153.82
Al III	28.45	Al VI	190.49

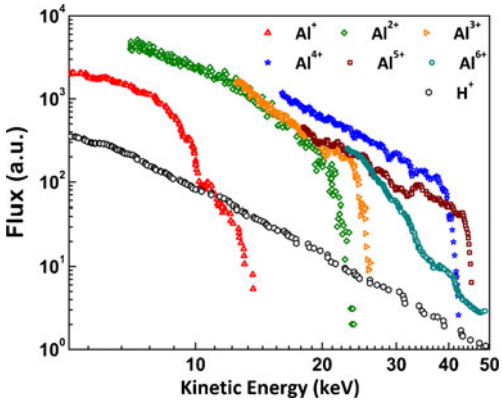

Figure 3. Kinetic energy spectrum of proton and other Al ions derived from the TPS image. Sudden change in the slope of each spectrum is the signature of having more than one temperature.

where k_B is the Boltzmann constant, $e = 2.71828....$, ε_0 is the free space permittivity, n_{eh} is the hot electron density and T_{eh} is the hot electron temperature.

Massive ions, accelerated in the sheath field preferentially along the target normal direction with an acceleration a, given by

$$a = \frac{q}{m}\sqrt{\frac{2k_B n_{eh} T_{eh}}{e\varepsilon_0}}. \tag{10}$$

Protons, which have the maximum charge-to-mass ratio form the fist set of ions that are accelerated, experience the maximum sheath and maximum acceleration. Heavier ions take larger time to travel and as the sheath potential changes with the departure of the lighter ions, the acceleration potential experienced is significantly smaller. The kinetic energy spectra of the ions derived from the TPS image is shown in figure 3. The sharp cut-off at the highest energy end of each ion spectrum, a typical signature of laser-accelerated ions from solids, is proportional to the maximum sheath field experienced by that ion. It is to be noted that the highest cut-off energy gradually decreases from H^+ to Al^{6+}, Al^{5+} and so on. Al^+ which has the least q/m (in the present experiment) gets least acceleration. The cut-off at the low energy end of each spectrum comes from the finite and circular active area of the MCP. Since the low-energy ions get maximum deflection, they are deflected out of the detector's active area.

5. Resolution

Experimental TPS trace width is a convolution of the instrumental function and the intrinsic width of the ions at the source. The trace width due to instrumental effects depends on the size of the extraction aperture and spatial resolution of the position-sensitive detector. In the present case, the channel of the MCP is about 12 μm in diameter. However, the electrons which generate fluorescence on the phosphor screen gives an additional width

giving an overall spatial resolution of about 100 μm. So, a single ion incident on the MCP makes a 100 μm spot. The finite size of the extraction aperture samples an ion beam at the entry of the TPS. This aperture largely determines the resolution. If the aperture is large, a more divergent ion beam is imaged in the spectrometer and the trace width is correspondingly larger. Larger aperture also leads to larger central bright spot formed by signal due to the photons impinging on the detector. The extraction aperture should be optimum such that the ion detection in the image is with a good signal-to-noise ratio. The instrumental width is smaller than the intrinsic width due to the divergence in the beam. Here, we used a 100 μm aperture, which provides very good charge resolution and enough signals for measuring the ion spectrum for a single laser pulse. Space-charge repulsion is one of the large contributors to the ion beam divergence and the trace width measured in the current spectrometer is limited by its influence. In typical laser–solid interactions, the emitted ion flux is generally very high (10^{10}–10^{11} ions per laser shot). Owing to its Maxwellian energy distribution, the density of low-energy ions is larger compared to the high-energy ions. The low-energy ions are affected much more by the space-charge field in the source region as well as in the traversal through the spectrometer to the detector. This is very clear in the measured ion image where the traces are well-resolved for the high-energy component of the ions (close to the origin) and they tend to diverge and overlap for low-energy ions towards the edge of the detector (figure 2a). In the measured traces, the width of the ion traces depends on the ion energy alone. The dependence of the trace width with ion energy is shown in figure 4. Beyond 30 keV, the trace width is seen to approach a limiting value. It is clear that the trace width is not limited by the instrumental function and the intrinsic larger divergence of the low-energy ions is discernible and their resolution is space-charge limited in our TPS. A polynomial fit to the trace width shows its functional dependence on ion energy as proportional to $\varepsilon^{-2/3}$. This is a typical characteristic of the ion divergence due to space-charge Coulomb repulsion and the present results correlate well with this scenario [23].

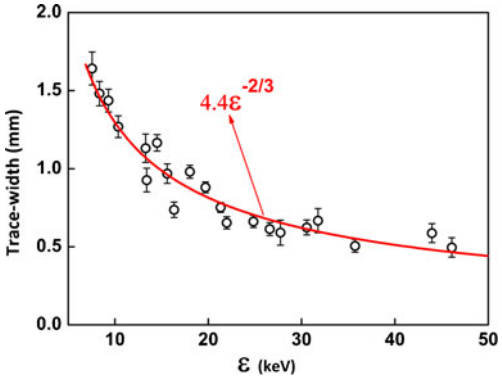

Figure 4. The dependence of parabolic trace width on ion energy. At lower ion energy, the trace width is broader and gradually trace width decreases as the ion energy is increased. Beyond 30–40 keV it reaches a limiting value of 0.6 mm. A non-linear curve-fitting yielded $\varepsilon^{-2/3}$ dependence of the trace width on ion energy.

6. Conclusion

A Thomson parabola ion spectrometer has been developed to study the laser-accelerated ions from solids. We present charge-resolved kinetic energy spectra and charge state propensity distribution of aluminum ions along with proton at an incident laser intensity of 10^{17} W/cm^2. Unlike laser–cluster interactions where highly charged ions are produced with very high average charge, laser–solid interactions produce relatively lower charged ions with low average charge. The resolution of the TPS is optimized such that ion image is obtained for a single laser pulse interaction. The width of the parabolic trace is shown to vary only with the ion energy. Smaller the ion energy, larger is the width and the width tends to become constant for higher ion energies. The larger trace width for low-energy ions is identified to be due to the ion divergence by the space-charge effect. The trace width is shown to vary with ion energy as $\varepsilon^{-2/3}$ which correlates to the well-established formalism for the ion divergence due to the space-charge effects. The use of MCP as the position-sensitive detector gives us the ability to measure the ion image online, immediately after the laser shot. Although the lower energy ion data is provided to demonstrate the good charge resolution achieved even at low ion energies, this TPS is designed to detect multi-MeV ions.

References

[1] S-W Bahk, P Rousseau, T A Planchon, V Chvykov, G Kalintchenko, A Maksimchuk, G A Mourou and V Yanovsky, *Opt. Lett*. **29**, 2837 (2004)
[2] G Ravindra Kumar, *Pramana – J. Phys.* **73**, 113 (2009)
[3] R Rajeev, T Madhu Trivikram, K P M Rishad, V Narayanan, E Krishnakumar and M Krishnamurthy, *Nature Phys.* **9**, 185 (2013)
[4] R Rajeev, T Madhu Trivikram, K P M Rishad, V Narayanan and M Krishnamurthy, *New J. Phys*. **15**, 043036 (2013)
[5] J Faure, Y Glinec, A Pukhov, S Kiselev, S Gordienko, E Lefebvre, J P Rousseau, F Burgy and V Malka, *Nature* **431**, 541 (2004)
[6] K Krushelnick, E L Clark, Z Najmudin, M Salvati, M I K Santala, M Tatarakis, A E Dangor, V Malka, D Neely, R Allott and C Danson, *Phys. Rev. Lett*. **83**, 737 (1999)
[7] A Maksimchuk, S Gu, K Flippo, D Umstadter and V Yu Bychenkov, *Phys. Rev. Lett*. **84**, 4108 (2000)
[8] S C Wilks, A B Langdon, T E Cowan, M Roth, M Singh, S Hatchett, M H Key, D Pennington, A MacKinnon and R A Snavely, *Phys. Plasmas* **8**, 542 (2001)
[9] Hiroyuki Daido, Mamiko Nishiuchi and Alexander S Pirozhkov, *Rep. Prog. Phys*. **75**, 056401 (2012)
[10] Victor Malka, Sven Fritzler, Erik Lefebvre, Emmanuel d Humires, Rgis Ferrand, Georges Grillon, Claude Albaret, Samuel Meyroneinc, Jean-Paul Chambaret, Andre Antonetti and Danile Hulin, *Med. Phys*. **31**, 1587 (2004)
[11] R A Snavely, M H Key, S P Hatchett, T E Cowan, M Roth, T W Phillips, M A Stoyer, E A Henry, T C Sangster, M S Singh, S C Wilks, A MacKinnon, A Offenberge, D M Pennington, K Yasuike, A B Langdon, B F Lasinski, J Johnson, M D Perry and E M Campbell, *Phys. Rev. Lett.* **85**, 2945 (2000)
[12] Paul Drake, *High-energy-density-physics* (Springer Verlag, Berlin Heidelberg, 2006)
[13] P Mora, *Phys. Rev. Lett*. **90**, 185002 (2003)

[14] M Murakami, Y-G Kang, K Nishihara, S Fujioka and H Nishimura, *Phys. Plasmas* **12**, 062706 (2005)
[15] M Passoni, V T Tikhonchuk, M Lontano and V Yu Bychenkov, *Phys. Rev. E* **69**, 026411 (2004)
[16] S Bagchi, P Prem Kiran, M K Bhuyan, S Bose, P Ayyub, M Krishnamurthy and G R Kumar, *Appl. Phys. Lett*. **90**, 141502 (2007)
[17] S Bagchi, P Prem Kiran, M K Bhuyan, S Bose, P Ayyub, M Krishnamurthy and G R Kumar, *Appl. Phys. B* **88**, 167 (2007)
[18] K Harres, M Schollmeier, E Brambrink, P Audebert, A Blažević, K Flippo, D C Gautier, M Geißel, B M Hegelich, F Nürnberg, J Schreiber, H Wahl and M Roth, *Rev. Sci. Instrum*. **79**, 093306 (2008)
[19] I W Choi, C M Kim, J H Sung, T J Yu, S K Lee, I J Kim, Y-Y Jin, T M Jeong, N Hafz, K H Pae, Y-C Noh, D-K Ko, A Yogo, A S Pirozhkov, K Ogura, S Orimo, A Sagisaka, M Nishiuchi, I Daito, Y Oishi, Y Iwashita, S Nakamura, K Nemoto, A Noda, H Daido and J Lee, *Rev. Sci. Instrum.* **80**, 053302 (2009)
[20] J T Morrison, C Willis, R R Freeman and L Van Woerkom, *Rev. Sci. Instrum*. **82**, 033506 (2011)
[21] R Rajeev, K P M Rishad, T Madhu Trivikram, V Narayanan and M Krishnamurthy, *Rev. Sci. Instrum*. **82**, 083303 (2011)
[22] Th Fennel, K-H Meiwes-Broer, J Tiggesbäumker, P-G Reinhard, P M Dinh and E Suraud, *Rev. Mod. Phys*. **82**, 1793 (2010)
[23] M S Benilov, *Plasma Sources Sci. Technol*. **18**, 014005 (2009)